Influence of dielectric materials on uniformity of large-area capacitively coupled plasmas for N_2/Ar discharges*

Ying-Shuang Liang(梁英爽), Yu-Ru Zhang(张钰如), and You-Nian Wang(王友年)†

School of Physics and Optoelectronic Technology, Dalian University of Technology, Dalian 116024, *China*

(Received 11 May 2016; revised manuscript received 29 June 2016; published online 25 August 2016)

The effect of the dielectric ring on the plasma radial uniformity is numerically investigated in the practical 450-mm capacitively coupled plasma reactor by a two-dimensional self-consistent fluid model. The simulations were performed for N_2/Ar discharges at the pressure of 300 Pa, and the frequency of 13.56 MHz. In the practical plasma treatment process, the wafer is always surrounded by a dielectric ring, which is less studied. In this paper, the plasma characteristics are systematically investigated by changing the properties of the dielectric ring, i.e., the relative permittivity, the thickness and the length. The results indicate that the plasma parameters strongly depend on the properties of the dielectric ring. As the ratio of the thickness to the relative permittivity of the dielectric ring increases, the electric field at the wafer edge becomes weaker due to the stronger surface charging effect. This gives rise to the lower N_2^+ ion density, flux and N atom density at the wafer edge. Thus the homogeneous plasma density is obtained by selecting optimal dielectric ring relative permittivity and thickness. In addition, we also find that the length of the dielectric ring should be as short as possible to avoid the discontinuity of the dielectric materials, and thus obtain the large area uniform plasma.

Keywords: capacitive N_2/Ar discharge, fluid simulation, dielectric materials, plasma radial uniformity

PACS: 52.50.Qt, 52.65.–y, 52.25.Mq **DOI:** 10.1088/1674-1056/25/10/105206

1. Introduction

Capacitively coupled plasmas (CCPs) have been extensively utilized in the semiconductor industry for thin film deposition and material etching of wafers.[1,2] The traditional 300 mm wafers for the semiconductor industry will be gradually replaced by the 450-mm ones, and accordingly the large-area capacitive plasma sources have attracted growing interest.[3] In order to ensure the same deposition or etching efficiency over the entire wafer in the course of practical processing and fabrication, the plasma density and the ion flux towards the wafers are expected to be homogeneous along the radial direction. However, the increase of the wafer size is more likely to exacerbate the difficulties in obtaining the homogeneous plasmas. Therefore, the control of the plasma uniformity over the entire wafer is one of the major challenges for the design of plasma systems.

The plasma uniformity is influenced by many factors, which can be broadly separated into three categories: the working gas (e.g., pressure and composition), the driven source (e.g., rf frequency and discharge power), and the reactor geometry (e.g., the electrode shape and material property). In capacitive discharges, when the frequency is not too high, such as 13.56 MHz, the plasma radial uniformity is compromised by the electrostatic edge effect. How to suppress the edge effect and obtain homogeneous plasmas have been the subject of intense research. Our previous work showed both theoretically and experimentally that the edge effect could be effectively suppressed and the more uniform plasma was obtained by properly decreasing the rf power or enlarging the electrode gap.[4,5] Furthermore, Xu *et al.* studied the phase-shift effect on the CCP discharge, especially on the radial uniformity of the plasma density and the ion flux.[6] They found that the edge effect could be controlled by adjusting the phase difference.

In addition, the dielectric materials also have an important influence on the plasma uniformity, and have been employed in the design of plasma reactors. Yang *et al.* utilized the graded conductivity electrode with a multilayer of dielectrics on it, and they found that the radial uniformity of the plasma and the ion flux in the sheath became better than in the case with the traditional flat electrode.[3] By means of a self-consistent fluid model, Bi *et al.* revealed that blocking the electrodes with dielectrics was an effective method to suppress the edge effect, thereby increasing the plasma uniformity.[7] Moreover, in Michna's work, multi-tile systems with neighboring tiles out of phase was proposed for obtaining good deposition uniformity in plasma enhanced chemical vapor deposition (PECVD) processes.[8] In the presence of dielectrics, the ions and electrons are accumulated on the dielectric surface, which is the so-called "surface-charging effect". The property (i.e., relative permittivity) and the geometrical size (i.e., thickness and length) of the dielectric affect the accumulated charge density, and therefore influence the potential on the dielectric surface.

*Project supported by the National Natural Science Foundation of China (Grant Nos. 11335004 and 11405019) and the Important National Science and Technology Specific Project of China (Grant No. 2011ZX02403-001).

†Corresponding author. E-mail: ynwang@dlut.edu.cn

© 2016 Chinese Physical Society and IOP Publishing Ltd

Due to the "surface-charging effect", an electric field with opposite direction is built up, and it has a significant influence on the plasma behavior, especially on the plasma uniformity. Compared with the working gas and the driven source, the dielectric material has less effect on the plasma density magnitude, but it significantly changes the plasma density profile. This is important for the uniformity of the etching and deposition, especially in large-scale plasma processing applications.

In the plasma treatment process, a dielectric ring (e.g., silicon dioxide and alumina ceramics) is used to fix the wafer and to suppress or weaken the edge effect. However, in the previous research mentioned above, the investigation of the dielectric ring effect on the plasma uniformity is limited, i.e., the working gas is simple (such as Ar), and the discharge reactor is simplified. Therefore, it is of great importance to well understand the effect of the dielectric ring on the plasma parameters in large-area actual reactors with complex gas mixtures. The emphasis of this work is on the influence of the dielectric ring on the plasma uniformity in large-area N_2/Ar capacitive discharges, which can help us to improve the uniformity in the plasma processing applications.

This paper is organized as follows. The fluid model is presented in Section 2. In Section 3, by changing the property of the dielectric ring, i.e., the relative permittivity, the thickness and the length, the plasma characteristics are investigated systematically. Finally, a brief summary is given in Section 4.

2. Description of the fluid model

2.1. Plasma equations

In recent years, Wang and his group developed a software platform for Multi-physics Analysis of Plasma Sources (MAPS), which contains three models, i.e., the fluid model,[4–6,9–11] the Particle-In-Cell/Monte Carlo (PIC/MC) model[8,12–15] and the global model.[16] The MAPS can be used to investigate the plasma behaviors in CCP and inductively coupled plasma (ICP) discharges. In this work, the fluid model is employed to study the N_2/Ar CCP discharge, in which 4 charged species (Ar^+, N_2^+, N^+ and electrons) and 5 neutral species (Ar metastable, the ground-state N atom, and the excited-state N_2 ($A^3\Sigma_u$), N_2 ($B\,^3\Pi_g$), N_2 ($a'\,\Sigma_u$) molecules) are considered. Various chemical reactions between the electrons, ions and neutral species are listed in Table 1 and Table 2. Ar_m, N_2 (A), N_2 (B), and N_2 (a′) are used to indicate the Ar metastable and three excited N_2 molecules.

Table 1. Overview of the chemical reactions for electrons taken into account in the model.

No.	Reaction	Rate coefficient/cm$^3\cdot$s^{-1}	Threshold	Ref.
1.1	$Ar+e\rightarrow Ar^+ +2e$	$2.34\times10^{-8}(T_e)^{0.59}\exp(-17.44/T_e)$	15.76	[2]
1.2	$Ar+e\rightarrow Ar_m+e$	$2.48\times10^{-8}(T_e)^{0.33}\exp(-12.78/T_e)$	11.55	[2]
1.3	$Ar_m+e\rightarrow Ar^+ +2e$	$6.8\times10^{-9}(T_e)^{0.67}\exp(-4.2/T_e)$	4.43	[2]
1.4	$N_2+e\rightarrow N_2^+ +2e$	$7.76\times10^{-9}(T_e)^{0.79}\exp(-16.75/T_e)$	15.60	[4]
1.5	$N+e\rightarrow N^+ +2e$	$3.87\times10^{-9}(T_e)^{0.86}\exp(-14.62/T_e)$	14.54	[4]
1.6	$N_2+e\rightarrow N^+ +N+2e$	$2.90\times10^{-9}(T_e)^{0.72}\exp(-29.71/T_e)$	18.0	[4], [17]
1.7	$N_2+e\rightarrow N_2(A)+e$	$8.06\times10^{-10}(T_e)^{-0.306}\exp(-8.87/T_e)$	6.17	[4]
1.8	$N_2+e\rightarrow N_2(B)+e$	$1.56\times10^{-8}(T_e)^{-0.52}\exp(-9.16/T_e)$	7.35	[4]
1.9	$N_2+e\rightarrow N_2(a')+e$	$6.6\times10^{-9}(T_e)^{-0.66}\exp(-11.05/T_e)$	8.40	[4]
1.10	$N_2+e\rightarrow N+N+e$	$2.15\times10^{-8}\exp(-14.39/T_e)$	9.75	[4]
1.11	$N_2^+ +e\rightarrow N+N$	$1.8\times10^{-7}(300/T_e)^{-0.39}$		[4]

In the fluid model, the plasma behaviors can be described by a series of fluid equations. For electrons, the density, flux and temperature can be obtained by solving Eqs. (1)–(3). Since the inertial term can be ignored due to the small electron mass, the electron flux is expressed as the drift-diffusion form.

$$\frac{\partial n_e}{\partial t}+\nabla\cdot\boldsymbol{\Gamma}_e=S_e, \tag{1}$$

$$\boldsymbol{\Gamma}_e=-\frac{1}{m_e\nu_{en}}\nabla(n_eT_e)-\frac{en_e}{m_e\nu_{en}}\boldsymbol{E}, \tag{2}$$

$$\frac{\partial[(3/2)n_eT_e]}{\partial t}=-\nabla\cdot\left(\frac{5}{2}T_e\boldsymbol{\Gamma}_e-\frac{5}{2}\frac{n_eT_e}{m_e\nu_{en}}\nabla T_e\right)-e\boldsymbol{E}\cdot\boldsymbol{\Gamma}_e-W_e, \tag{3}$$

Here, n_e, $\boldsymbol{\Gamma}_e$, m_e, and T_e are the density, flux, mass, and temperature of the electrons, respectively. $S_e=\sum_i k_in_1n_2$, is the source term, including the reactions that create and destroy electrons, where k_i, n_1, n_2 are the rate coefficients and particle densities. $W_e=\sum_j\varepsilon_jk_jn_1n_e$ is the electron energy loss term, and ε_j represents the threshold energy. ν_{en} is the electron–neutral collision frequency, and $\boldsymbol{E}$ is the electric field.

Since the ion temperature is assumed at $T_{gas}=300$ K based on the cold fluid approximation, only the continuity equation and momentum balance equation are needed for ions

$$\frac{\partial n_i}{\partial t}+\nabla\cdot(n_i\boldsymbol{u}_i)=S_i, \tag{4}$$

$$\frac{\partial(n_im_i\boldsymbol{u}_i)}{\partial t}+\nabla\cdot(n_im_i\boldsymbol{u}_i\boldsymbol{u}_i)=-\nabla p_i+en_i\boldsymbol{E}+\boldsymbol{M}_i, \tag{5}$$

where n_i, m_i, $\boldsymbol{u_i}$, p_i are the density, mass, velocity, and pressure of the ions, respectively. S_i is the source term. $\boldsymbol{M_i}$, the

momentum transfer term of the ions with neutral species, can be expressed as

$$\boldsymbol{M_i} = \frac{m_i m_n}{m_i + m_n} n_i \boldsymbol{u_i} \nu_{\text{in}},$$

where ν_{in} represents the collision frequency between the ions and neutral species.

The density of the neutral species is obtained by solving the continuity equation:

$$\frac{\partial n_n}{\partial t} + \nabla \cdot \boldsymbol{\Gamma_n} = S_n, \tag{6}$$

where n_n, $\boldsymbol{\Gamma_n}$, and S_n are the density, flux, and source term of neutral particles.

Under the conditions investigated in this paper, the induced electric field excited by the plasma is negligible. Thus only the electrostatic field is considered by solving the Poisson equation, and can be regarded as the total electric field $\boldsymbol{E}$ in Eq. (2).

$$\nabla^2 V = -\frac{e}{\varepsilon_0}\left(n_{\text{i}} - n_{\text{e}}\right), \tag{7}$$

$$\boldsymbol{E} = -\nabla V, \tag{8}$$

where V represents the electric potential, and ε_0 is the dielectric constant in a vacuum.

Table 2. Overview of the chemical reactions for ions and neutral species taken into account in the model.

No.	Reaction	Rate coefficient/cm$^3 \cdot$s^{-1}	Ref.
2.1	$Ar_m + Ar_m \rightarrow Ar^+ + Ar + e$	5.0×10^{-10}	[9]
2.2	$N_2(A) + N_2(a') \rightarrow N_2^+ + N_2 + e$	3.2×10^{-12}	[4]
2.3	$N_2(a') + N_2(a') \rightarrow N_2^+ + N_2 + e$	5.0×10^{-11}	[4]
2.4	$N_2(A) + N \rightarrow N_2 + N$	2.0×10^{-12}	[4]
2.5	$N_2(A) + N_2 \rightarrow N_2 + N_2$	3.0×10^{-18}	[4]
2.6	$N_2(A) + N_2(A) \rightarrow N_2(B) + N_2$	7.7×10^{-11}	[4]
2.7	$N_2(B) + N_2 \rightarrow N_2 + N_2$	1.5×10^{-12}	[4]
2.8	$N_2(B) + N_2 \rightarrow N_2(A) + N_2$	2.85×10^{-11}	[4]
2.9	$N_2(a') + N_2 \rightarrow N_2(B) + N_2$	1.9×10^{-13}	[4]
2.10	$N + N + N_2 \rightarrow N_2(B) + N_2$	$8.27 \times 10^{-34} \exp(500.0/T_{\text{gas}})$ (cm$^6 \cdot$s^{-1})	[4]
2.11	$N + N + N \rightarrow N_2 + N$	1.0×10^{-32} (cm$^6 \cdot$s^{-1})	[4]
2.12	$N_2(B) \rightarrow N_2(A) + h\nu$	2.0×10^{5} (s^{-1})	[4]
2.13	$Ar^+ + N_2 \rightarrow Ar + N_2^+$	4.45×10^{-10}	[18]
2.14	$Ar^+ + N \rightarrow Ar + N^+$	4.45×10^{-10}	[18]
2.15	$N_2^+ + Ar \rightarrow N_2 + Ar^+$	2.81×10^{-10}	[18]
2.16	$N_2(B) + Ar \rightarrow N_2(A) + Ar$	3.0×10^{-13}	[18]
2.17	$N_2(a') + Ar \rightarrow N_2(B) + Ar$	1.0×10^{-14}	[18]

2.2. Dielectric boundary

To solve Eqs. (1)–(8), appropriate boundary conditions (BCs) are needed. The schematic diagram of the CCP reactor used in this study is shown in Fig. 1. An Si wafer (45 cm in diameter and $h_1 = 0.08$ cm in thickness), surrounded by an L-shaped dielectric ring, sits in contact with the grounded lower metal electrode (50 cm in diameter). The relative permittivities of the wafer and the dielectric ring are $\varepsilon_{rw} = 12.5$ and ε_{rr}, respectively.

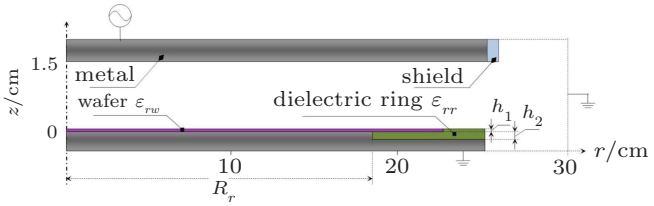


Fig. 1. (color online) Schematic diagram of the reactor configuration.

Since charges are accumulated at the dielectric surface due to the "surface-charging effect", as mentioned in Section 1, the potential at the plasma-wafer interface cannot be treated as that at the lower metal electrode (i.e., grounded). Moreover, it is observed from Fig. 1 that, a segment of the dielectric ring is sandwiched between the wafer and the lower metal electrode, which forms a two-layer dielectric structure. Therefore, the potential at the wafer edge is expected to be different from that at the central region. In order to obtain the plasma potential at the plasma-dielectric surface accurately, a general formula of the potential at the two-layer dielectric surface is given for the first time.

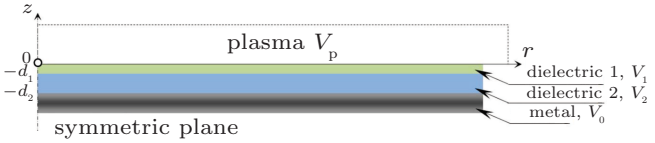


Fig. 2. (color online) Schematic diagram of the two-layer dielectric structure.

A typical two-layer dielectric structure is shown in Fig. 2. The first dielectric plate (with a thickness of d_1 and relative permittivity of ε_1) is placed above the second dielectric plate (with a thickness of $d_2 - d_1$ and relative permittivity of ε_2), and a metal plate is placed below them. The dielectric-plasma interface potential V_s is deduced as follows.

Since there are no free charges in the dielectrics, the potential in the first dielectric layer (V_1) and in the second layer (V_2) can be determined by the Laplace equation:

$$\nabla^2 V_i = 0, \quad (i = 1 \text{ or } 2). \tag{9}$$

Assuming that the diameter of the dielectric is much larger than its thickness, the problem rules out the radial variation, and only the axial variation is considered. Accordingly, equation (9) is simplified to be

$$\frac{\mathrm{d}^2 V_i}{\mathrm{d}z^2} = 0, \quad (i = 1 \text{ or } 2). \tag{10}$$

Due to the continuity of the potential at the dielectric interface, we get

$$\begin{cases} V_1\big|_{z=0} = V_\mathrm{s} \\ V_1\big|_{z=-d_1} = V_2\big|_{z=-d_1}, \\ V_2\big|_{z=-d_2} = V_0 \end{cases} \tag{11}$$

where V_0 is the potential at the lower metal electrode. Since the ions and the electrons rapidly charge up at the dielectric surface, the potential at $z = 0$ has to satisfy the generalized Gauss law:

$$\left(\varepsilon_1 \frac{\mathrm{d}V_1}{\mathrm{d}z} - \frac{\mathrm{d}V_\mathrm{p}}{\mathrm{d}z}\right)\bigg|_{z=0} = \frac{\sigma_t}{\varepsilon_0}. \tag{12}$$

Here, V_p is the plasma potential. σ_t in Eq. (12) represents the surface charge density, and it is obtained by integrating the flux over time, i.e.,

$$\sigma_t = \int_0^t e(\boldsymbol{\Gamma}_\mathrm{i} - \boldsymbol{\Gamma}_\mathrm{e})\,\mathrm{d}t.$$

Similarly, at $z = -d_1$,

$$\varepsilon_1 \frac{\mathrm{d}V_1}{\mathrm{d}z}\bigg|_{z=-d_1} = \varepsilon_2 \frac{\mathrm{d}V_2}{\mathrm{d}z}\bigg|_{z=-d_1}. \tag{13}$$

Substituting the BCs (11)–(13) into Eq. (10), V_s is expressed as

$$V_\mathrm{s} = \left(V_\mathrm{p} + \frac{\Delta z \sigma_t}{\varepsilon_0} + \frac{\Delta z}{a} V_0\right) \Bigg/ \left(1 + \frac{\Delta z}{a}\right), \tag{14}$$

where $a = d_1/\varepsilon_1 + (d_2 - d_1)/\varepsilon_2$.

Since the upper electrode is powered by an rf source, and the lower electrode together with the side wall is grounded in this paper, the BCs of the potential at the dielectric-plasma interface can be expressed as:

$$V_\mathrm{s} = \begin{cases} \left(V_\mathrm{p} + \dfrac{\Delta z \sigma_t}{\varepsilon_0}\right) \Big/ \left(1 + \dfrac{\Delta z}{h_1/\varepsilon_{rw}}\right), & (0\ \mathrm{cm} \le r \le R_r), \\ \left(V_\mathrm{p} + \dfrac{\Delta z \sigma_t}{\varepsilon_0}\right) \Big/ \left(1 + \dfrac{\Delta z}{h_1/\varepsilon_{rw} + h_2/\varepsilon_{rr}}\right), & (R_r < r \le 22.5\ \mathrm{cm}), \\ \left(V_\mathrm{p} + \dfrac{\Delta z \sigma_t}{\varepsilon_0}\right) \Big/ \left(1 + \dfrac{\Delta z}{(h_1 + h_2)/\varepsilon_{rr}}\right), & (22.5\ \mathrm{cm} < r \le 25.0\ \mathrm{cm}). \end{cases} \tag{15}$$

Here, R_r is defined as the distance from the central axis to the left edge of the dielectric ring along the radial direction.

Besides, other BCs, which are also needed to complete the model, have been described previously in Ref. [4]. So a brief description is here. The ion densities are assumed to be continuous at the walls and the axial, i.e., $\nabla n_\mathrm{i} = 0$. Since the neutral species are considered to be lost at the walls with a surface-loss probability β_n in the simulation, the BCs for the neutral species continuity equation are given by

$$\boldsymbol{\Gamma}_n = \frac{\beta_n}{2(2 - \beta_n)} \times n_n \upsilon_{\mathrm{th},n}, \tag{16}$$

where $\upsilon_{\mathrm{th},n}$ is the thermal velocity of the neutral species. The excited Ar atoms and N_2 molecules (N_2 (A), N_2 (B), and N_2 (C) are supposed to be completely absorbed at the walls,[19] i.e., β_n=1. The N atom surface-loss probability is assumed to be 0.008.[20] As for the electron continuity equation, the BC is not necessary due to the discrete schemes adopted in the model.

3. Results and discussion

To understand the influences of the dielectric ring on the plasma characteristics, the simulations were performed in N_2/Ar (0.1/0.9) plasmas at the pressure of 300 Pa, with the frequency of 13.56 MHz and voltage of 50 V. In addition to the previous description of the reactor in Section 2, some other details about the reactor are added here. The radius of the reactor is 30 cm, and the gap between the wafer and the upper electrode is 1.5 cm. Unless otherwise specified, the dielectric ring is made of silica ($\varepsilon_{rr} = 3.9$ and thickness $h_1 + h_2 = 0.98$ cm), and the distance from the central axis to the left edge of the dielectric ring R_r is 18.8 cm.

3.1. Effects of the dielectric ring relative permittivity

In this part, the plasma parameters are examined with different dielectric rings, i.e., silicon (Si), ceramic alumina (Al_2O_3) and silica (SiO_2), whose relative permittivities are 12.5, 8.5, and 3.9, respectively.

Radial profiles of the N_2^+ ion density along the mid-gap

between electrodes (i.e., $z = 0.75$ cm, $r = 0 - 30$ cm) and the axial N_2^+ ion flux towards the wafer surface (i.e., $z = 0$ cm, $r = 0 - 22.5$ cm) with different ε_{rr} are presented in Figs. 3 and 4. It is obvious that the N_2^+ ion density and the flux at the wafer center (i.e., $r < 15$ cm) are quite uniform and almost constant for all ε_{rr}, which means the dielectric ring has no significant influence on the plasma properties at the central region. Whereas, the N_2^+ ion density and the flux at the wafer edge behave differently with different ε_{rr}. The radial profile of the N_2^+ ion density is characterized by a tiny bump near the electrode edge (i.e., $r = 24$ cm). The N_2^+ flux first increases along the radial direction at 15 cm$< r < R_r$ (18.8 cm), then there is a significant drop at $r = R_r$, and finally it increases again at $R_r < r < 22.5$ cm. Besides, both the ion density and the flux at the wafer edge increase with ε_{rr}, due to the strong electric field at large ε_{rr} (as shown in Fig. 6(b)).

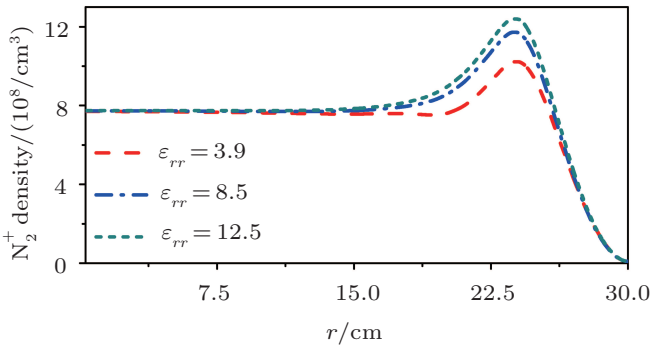


Fig. 3. (color online) Radial distributions of the N_2^+ density along the mid-gap between electrodes (z=0.75 cm) with different dielectric ring relative permittivities.

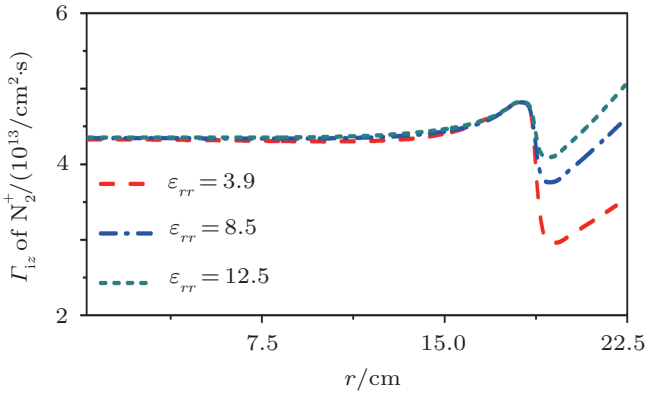


Fig. 4. (color online) Radial distributions of the axial flux of N_2^+ on the wafer ($z = 0$ cm) with different dielectric ring relative permittivities.

In practical processes, N atoms are also very important, as they are responsible for the film deposition. Fig. 5 illustrates spatial distributions of the N atom density at different ε_{rr}. The results indicate that the evolution of the N atom density with ε_{rr} is similar to the N_2^+ ion density. The peak of the N density increases from $2.8 \times 10^{11}/cm^3$ to $3.6 \times 10^{11}/cm^3$ when ε_{rr} increases from 3.9 to 12.5.

The non-uniform distribution of the axial N_2^+ ion flux is caused by the discontinuity of the dielectric materials. This phenomenon has also been observed in previous research though under different discharge conditions.[21] Indeed, part of the dielectric ring is sandwiched between the wafer and the lower electrode (cf. Fig. 1). Hence, the surface charge density and the electric field above the wafer here (i.e., $R_r < r < 22.5$ cm) are different from those at the central region (i.e., $r < 15$ cm), and this gives rise to the different plasma properties. In order to highlight the different plasma parameters at the wafer edge, the surface charge density and the axial electric field in the range of $R_r < r < 22.5$ cm are shown in Fig. 6. From Fig. 6(a), it is clear that less negative charges are accumulated at the wafer edge at larger ε_{rr}. At the wafer center, the surface charge density is almost constant with low values (not shown here), because the wafer is very thin.

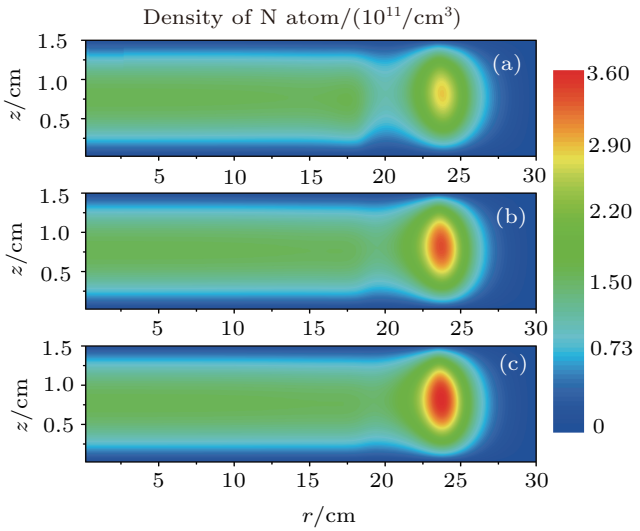


Fig. 5. (color online) Spatial distributions of the N density with different dielectric ring relative permittivities: (a) $\varepsilon_{rr} = 3.9$, (b) $\varepsilon_{rr} = 8.5$, (c) $\varepsilon_{rr} = 12.5$.

From Fig. 6(b), it is observed that the electric field at the wafer edge increases along the radial direction due to the edge effect, and therefore the plasma density and the ion flux increase with the radial distance at the wafer edge, as shown in Figs. 3–5. Since the so-called "surface-charging effect" is more remarkable at the wafer edge, the induced electric field in the dielectric materials (E_{zr}) weakens the axial electric field in the plasma more effectively. Therefore, the electric field at the center (not shown here) is stronger than at the wafer edge, and this gives rise to a rapid drop in the axial N_2^+ ion flux at R_r. However, the drop in the plasma density at R_r is less obvious, due to the diffusion. Since E_{zr} is proportional to the ratio of the surface charge density to the dielectric relative permittivity, E_{zr} becomes weaker at larger ε_{rr}, leading to the stronger electric field on the wafer. As a result, both the plasma density and the axial ion flux at the wafer edge increase with ε_{rr}, as shown in Figs. 3–5. When ε_{rr} is large, the stronger axial electric field at the wafer edge results in a higher plasma density, which indicates worse uniformity. However, the discontinuity in the ion flux becomes less obvious at larger ε_{rr}. Hence, the

dielectric ring material needs to be chosen carefully to satisfy the specific requirements in actual production processes.

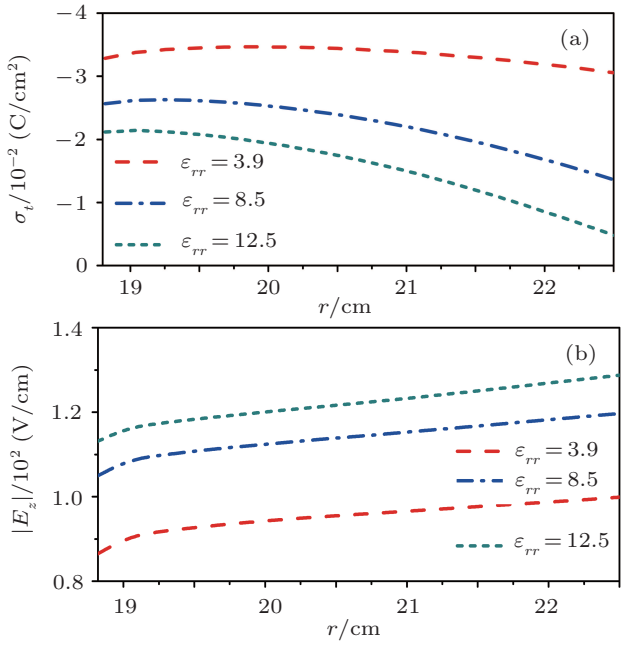


Fig. 6. (color online) Radial distributions of (a) the accumulated charge density and (b) the axial electric field at the wafer edge (i.e., $z=0$ cm and $R_r < r < 22.5$ cm) with different dielectric ring relative permittivities. In panel (a), the minus sign (–) scale on the vertical axis indicates negative charge accumulation.

3.2. Effects of the dielectric ring thickness

In order to study the influence of the dielectric ring thickness on the plasma parameters, h_2 varies from 0.1 cm to 0.9 cm, with ε_{rr} fixed at 3.9. Since the dielectric ring thickness has little effect on the plasma behavior at the central region, only the parameters at the wafer edge are shown here. Fig. 7(a) shows the radial distribution of the potential on the wafer (V_s) in the range of $R_r < r < 22.5$ cm at different h_2. It is clear that V_s increases along the radial direction, and a higher V_s is obtained with a thicker dielectric ring. This is because the wafer and the dielectric ring can be treated as two parallel plate capacitors which are connected in series, and the capacitance of the dielectric ring (and the wafer) is in inverse proportion to its thickness h_2 (and h_1) and the potential difference between the upper and lower surfaces. Hence, for the "capacitor system", there is a positive correlation between the thickness and the potential difference between the upper and lower surfaces. In other words, with a constant h_1, the potential difference between the upper surface of the wafer and the lower surface of the dielectric ring, which is equivalent to V_s, increases with h_2.

The electric field on the wafer surface at the edge is plotted in Fig. 7(b). It is clear that the electric field increases gradually along the radial direction due to the edge effect, and it decreases with the increasing dielectric ring thickness due to the surface charging effect. By comparing Figs. 6(b) and 7(b), it is clear that the evolution of the electric field with the dielectric ring thickness is in contrast to that with the dielectric ring permittivity. This can be simply interpreted as the inverse relationship between the dielectric ring thickness and the permittivity in the capacitor system. This can also be understood by examining the potential distribution at and above the wafer. Although the potential above the wafer (not shown here) increase with h_2, the potential at the wafer surface increases faster. Therefore,we can conclude from Eq. (8) that the axial electric field at the wafer surface decreases with the ring thickness. The higher potential corresponding to a lower electric field was also observed in Ref. [3], by using the segmented dielectric electrodes.

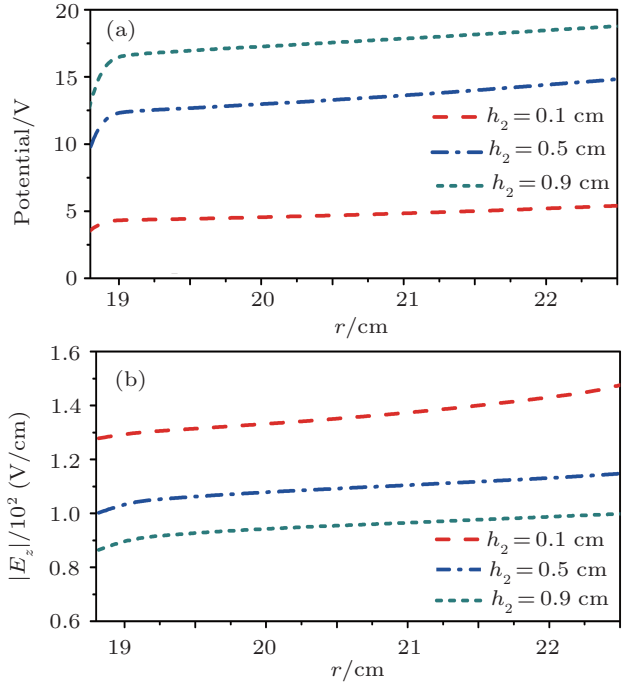


Fig. 7. (color online) Radial distributions of (a) the electric potential and (b) the axial electric field at the wafer edge (i.e., $z=0$ cm and $R_r < r < 22.5$ cm) with different dielectric ring thicknesses.

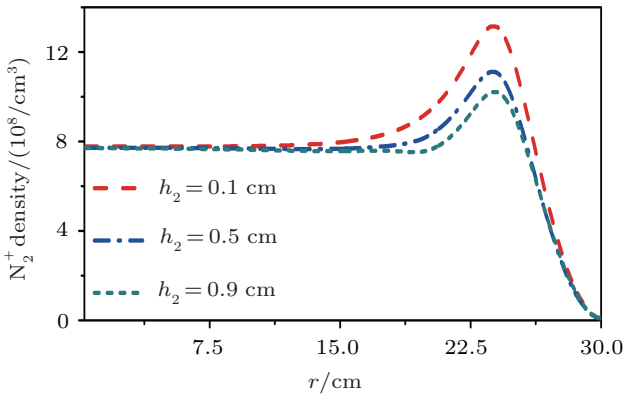


Fig. 8. (color online) Radial distributions of the N_2^+ density along the midgap between electrodes ($z=0.75$ cm) with different dielectric ring thicknesses.

Since the electric field in the plasma at the edge is stronger when the dielectric ring is thinner, higher N_2^+ ion density and ion flux are obtained under this condition, as is

clear from Figs. 8 and 9. Similarly, the peak of the N atom density at the radial edge descends significantly when h_2 increases to 0.9 cm (not shown here), and the radial uniformity of the plasma density becomes better due to the weaker edge effect.

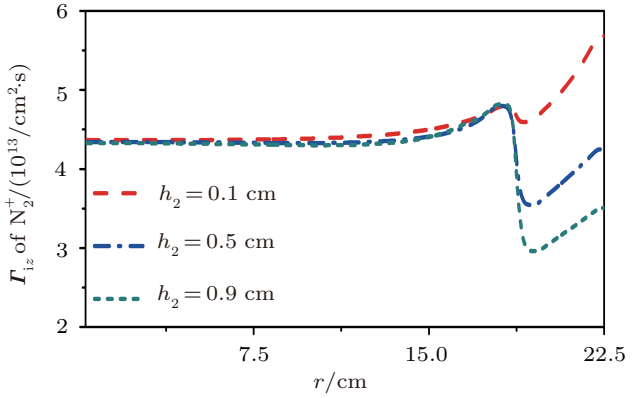


Fig. 9. (color online) Radial distributions of the axial flux of N_2^+ on the wafer ($z = 0$ cm) with different dielectric ring thicknesses.

3.3. Effects of the dielectric ring length

From the results discussed above, it is clear to see the discontinuity in the ion flux at R_r. In this subsection, the effect of the dielectric ring length on the discharge is investigated to improve the ion flux distribution, by changing R_r in the range of 0 cm to 18.8 cm. Note that $R_r = 0$ cm indicates that the entire SiO_2 dielectric ring is sandwiched between the wafer and the metal electrode, as shown in Fig. 10.

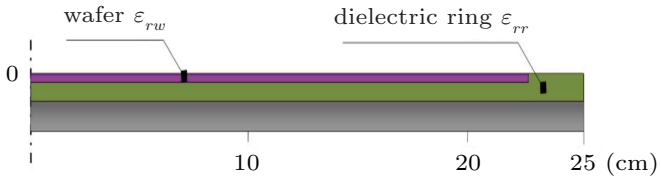


Fig. 10. (color online) Schematic diagram of the entire-layer dielectric ring case ($R_r = 0$ cm).

Radial distributions of the N_2^+ ion density along the mid-gap between electrodes, and the axial flux of the N_2^+ ion on the wafer at different R_r are plotted in Figs. 11 and 12. It is obvious that the dielectric ring length exercises a great influence on the plasma parameters. The results in the case of $R_r = 18.8$ cm have been previously described in Subsections 3.1 and 3.2. As R_r is shortened to 10.5 cm, the ion density is lower than in the case of $R_r = 18.8$ cm. Moreover, the N_2^+ ion density first decreases to $5.0 \times 10^8/\text{cm}^3$ at about 15 cm, and then it increases along the radial direction. Apparently, the radial plasma uniformity is worse at this condition. This is because the stronger "surface-charging effect", due to the existence of the dielectric ring at $r > 10.5$ cm, weakens the electric field there, and results in the lower ion density. Moreover, abundant N_2^+ ions at the wafer center and the edge diffuse to the low density region, and this gives rise to the lower ion density at the central and edge areas than that of the case $R_r = 18.8$ cm. The evolution of the N atom density with R_r is similar to the ion density (cf. Fig. 13(b)). The radial distribution of the N_2^+ ion flux at $R_r = 10.5$ cm is similar to that of the case of $R_r = 18.8$ cm, except for the lower value and the radial position where the ion flux exhibits a rapid decrease, as shown in Fig. 12. On one hand, the lower ion flux is caused by the lower ion density. On the other hand, the significant reduction in the ion flux at $r = R_r$ demonstrates that the discontinuity of the dielectric materials affects the plasma properties remarkably. The results indicate that small R_r ($R_r > 0$ cm) leads to bad plasma radial uniformity. By enlarging R_r, a larger area of uniform plasma can be obtained, and this accordingly helps to improve the etching and deposition quality.

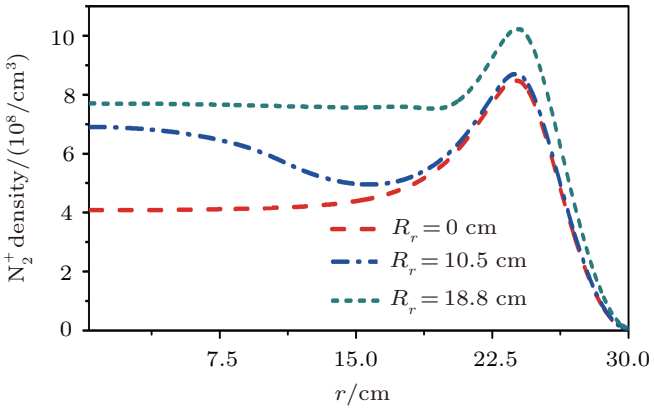


Fig. 11. (color online) Radial distributions of the N_2^+ density along the mid-gap between electrodes ($z = 0.75$ cm) with different R_r.

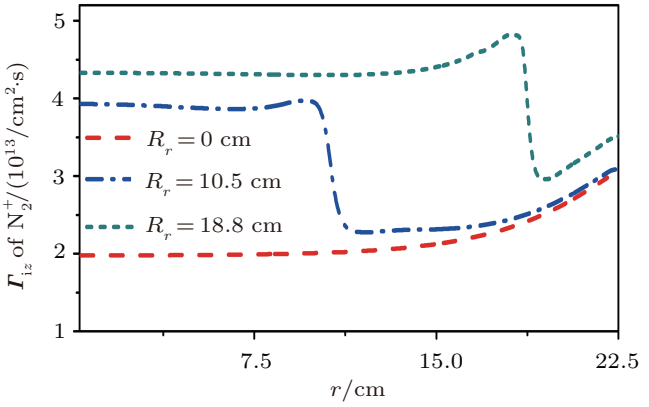


Fig. 12. (color online) Radial distributions of the axial flux of N_2^+ on the wafer ($z = 0$ cm) with different R_r.

For the case of $R_r = 0$ cm, which is similar to a dielectric barrier discharges,[2,22] the N_2^+ ion density and the N atom density at the central region are much lower than the other two cases (i.e., $R_r = 18.8$ cm and $R_r = 10.5$ cm), and they gradually increase along the radial direction. This is again because more negative charges are accumulated at the wafer center, and weaken the electric field there. Moreover, the ion flux on the wafer exhibits a strikingly different distribution, i.e., it shows a lower value at the center, and it increases monotonically along

the radial direction. This indicates that the discontinuity of the dielectrics is effectively eliminated, although the plasma density and the flux decrease to some extent.

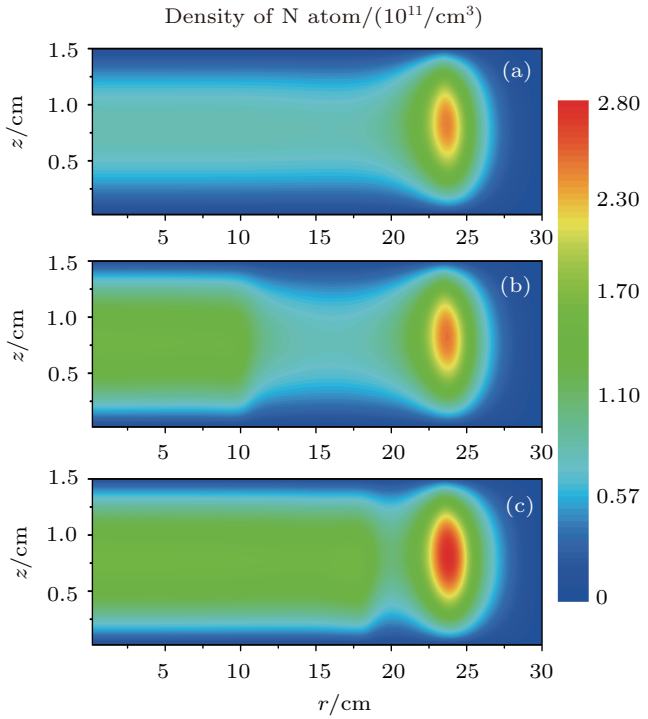


Fig. 13. (color online) Spatial distributions of the N density with different R_r: (a) $R_r = 0$ cm, (b) $R_r = 10.5$ cm, and (c) $R_r = 18.8$ cm.

4. Summary

In this paper, a two-dimensional self-consistent fluid model is employed to study the effects of the dielectric ring on the plasma characteristics, especially on the plasma uniformity, for a large-area N_2/Ar discharge. The results indicate that the plasma parameters strongly depend on the properties of the dielectric ring.

First, the effects of the relative permittivity and thickness (or the ratio of the thickness to the relative permittivity, i.e., h_2/ε_{rr}) of the dielectric ring have been investigated, and an important influence on the plasma parameters, especially at the wafer edge, has been observed. This is because when h_2/ε_{rr} is large, the electric field at the wafer edge becomes much weaker. This gives rise to the lower N_2^+ ion density, ion flux and N atom density there, and a better uniformity of the plasma density is obtained. Moreover, it is also observed that the radial distribution of the ion flux exhibits a rapid drop near the radial position of R_r, which is caused by the discontinuity of the dielectric materials. Although the entire-layer dielectric ring (i.e., $R_r = 0$ cm) helps to eliminate the discontinuity, the better uniformity is obtained at the expense of a drop in the production efficiency. From the results discussed above, the relative high plasma density and ion flux can be obtained by decreasing h_2/ε_{rr} of the dielectric ring. Therefore, by employing a dielectric ring with larger R_r and lower h_2/ε_{rr}, the larger area uniform plasma with a higher deposition or etching rate can be achieved.

References

[1] Chabert P and Braithwaite N 2011 *Physics of Ratio-Frequency Plasmas* (Cambridge University Press)
[2] Lieberman M A and Lichtenberg A J 2005 *Principles of Plasma Discharges and Materials Processing*, 2nd edn. (New York: Wiley-Interscience)
[3] Yang Y and Kushner M J 2010 *J. Appl. Phys.* **108** 113306
[4] Liang Y S, Liu Y X, Zhang Y R and Wang Y N 2015 *J. Appl. Phys.* **117** 083301
[5] Liu Y X, Liang Y S, Wen D Q, Bi Z H and Wang Y N 2015 *Plasma Sources Sci. Technol.* **24** 025013
[6] Xu X, Zhao S X, Zhang Y R and Wang Y N 2010 *J. Appl. Phys.* **108** 043308
[7] Bi Z H, Dai Z L, Zhang Y R, Liu D P and Wang Y N 2013 *Plasma Sources Sci. Technol.* **22** 055007
[8] Michna T and Ellingboe A R 2011 *Cur. Appl. Phys.* **11** S9
[9] Gao F, Liu W, Zhao S X, Zhang Y R, Sun C S and Wang Y N 2013 *Chin. Phys. B* **22** 115205
[10] Wang Y H, Liu W, Zhang Y R, Sun C S and Wang Y N 2015 *Chin. Phys. B* **24** 095203
[11] Xu H J, Zhao S X, Gao F, Zhang Y R, Li X C and Wang Y N 2015 *Chin. Phys. B* **24** 115201
[12] Liu Y X, Zhang Q Z, Liu J, Song Y H, Bogaerts A and Wang Y N 2013 *Plasma Sources Sci. Technol.* **22** 025012
[13] Zhang Q Z, Liu Y X, Jiang W, Bogaerts A and Wang Y N 2013 *Plasma Sources Sci. Technol.* **22** 025014
[14] Zhang Q Z, Wang Y N and Bogaerts A 2014 *J. Appl. Phys.* **115** 223302
[15] Wen D Q, Zhang Q Z, Jiang W, Song Y H, Bogaerts A and Wang Y N 2014 *J. Appl. Phys.* **115** 233303
[16] Liu W, Wen D Q, Zhao S X, Gao F and Wang Y N 2015 *Plasma Sources Sci. Technol.* **24** 025035
[17] Chanson R, Rhallabi A, Fernandez M C and Cardinaud C, Landesman J P 2013 *J. Vac. Sci. Technol. A* **31** 011301
[18] Bogaerts A 2009 *Spectrochim. Acta, Part B* **64** 126
[19] Sode M, Jacob W, Schwarz-Selinger T and Kersten H 2015 *J. Appl. Phys.* **117** 083303
[20] Adams S F, Miller T A 2000 *Plasma Sources Sci. Technol.* **9** 248
[21] Yagisawa T, Shimada T and Makabe T 2005 *J. Vac. Sci. Technol. B* **23** 2212
[22] Barjasteh A and Eslamia E 2016 *Phys. Plasmas* **23** 033506